Simultaneous Fat Suppression and Band Reduction with Large-Angle Multiple-Acquisition Balanced Steady-State Free Precession

Brady Quist,[1] Brian A. Hargreaves,[2] Tolga Cukur,[3] Glen R. Morrell,[4] Garry E. Gold,[2] and Neal K. Bangerter[1,4]*

Balanced steady-state free precession (bSSFP) MRI is a rapid and signal-to-noise ratio-efficient imaging method, but suffers from characteristic bands of signal loss in regions of large field inhomogeneity. Several methods have been developed to reduce the severity of these banding artifacts, typically involving the acquisition of multiple bSSFP datasets (and the accompanying increase in scan time). Fat suppression with bSSFP is also challenging; most existing methods require an additional increase in scan time, and some are incompatible with bSSFP band-reduction techniques. This work was motivated by the need for both robust fat suppression and band reduction in the presence of field inhomogeneity when using bSSFP for flow-independent peripheral angiography. The large flip angles used in this application to improve vessel conspicuity and contrast lead to specific absorption rate considerations, longer repetition times, and increased severity of banding artifacts. In this work, a novel method that simultaneously suppresses fat and reduces bSSFP banding artifact with the acquisition of only two phase-cycled bSSFP datasets is presented. A weighted sum of the two bSSFP acquisitions is taken on a voxel-by-voxel basis, effectively synthesizing an off-resonance profile at each voxel that puts fat in the stop band while keeping water in the pass band. The technique exploits the near-sinusoidal shape of the bSSFP off-resonance spectrum for many tissues at large (>50°) flip angles. Magn Reson Med 67:1004–1012, 2012. © **2011 Wiley Periodicals, Inc.**

Key words: bSSFP; SSFP; steady state; fat suppression; artifact reduction; flow-independent angiography

Balanced steady-state free precession (bSSFP) is a rapid and signal-to-noise ratio (SNR)-efficient imaging method, but suffers from characteristic bands of signal loss in regions of large field inhomogeneity. Several methods have been developed to reduce the severity of these banding artifacts, typically involving a penalty in scan time. Multiple phase-cycled bSSFP datasets can be acquired and combined in various ways (linear combination, maximum intensity, and sum of squares) to reduce the severity of banding, as described in Refs. 1–9. Another technique, wideband SSFP, utilizes two alternating repetition times (TR) with alternating radiofrequency phase to widen the band spacing in bSSFP, thereby reducing banding (10). Slow modulations in the spectral offset frequency have also been used to reduce banding (11).

Fat suppression with bSSFP is also challenging. Numerous suppression techniques have been proposed, including linear combination (12), transition to driven equilibrium (13), fluctuating equilibrium MRI (14), iterative decomposition of water and fat with echo asymmetry and least-squares estimation and other Dixon methods (15–17), phase-sensitive fat detection (18,19), alternating TR (20), and periodic fat saturation methods (21). However, most methods require an additional increase in scan time, and some are incompatible with bSSFP band-reduction techniques (12). Furthermore, these techniques have varying degrees of robustness to off-resonance, and some suffer from partial-volume effects (18,19). Some are transient techniques, relying on a transient magnetization preparation to suppress fat (13,21), whereas others work in the steady state (12,14,15,19).

This work was motivated by the need for both robust fat suppression and band reduction in the presence of field inhomogeneity when using bSSFP for flow-independent peripheral angiography (22,23). Relatively, large flip angles (~50° or larger) are desirable when using bSSFP for peripheral angiography to increase vessel conspicuity and improve contrast (24). Unfortunately, this can lead to SAR considerations and longer TR. As TR increases, the nulls in the SSFP spectral profile responsible for banding artifacts are more closely spaced in frequency. This can increase the number of signal null bands appearing in the image over a given range of off-resonance, while simultaneously making the transitions from signal to signal null more abrupt spatially; the bands of signal null get thinner and closer together, and consequently the edges get sharper. While the degree of band reduction is unaffected by TR, rapid spatial modulations in signal are typically less desirable than slower spatial modulations. These problems are exacerbated at higher field strengths (e.g., 3 T). Fat suppression can also be compromised for a number of the aforementioned techniques as TR increases (14,20). Ideally, we would like a bSSFP technique that robustly suppresses fat without partial-volume effects or artifacts, reduces bSSFP

[1]Department of Electrical and Computer Engineering, Brigham Young University, Provo, Utah, USA.

[2]Department of Radiology, Stanford University, Stanford, California, USA.

[3]Department of Electrical Engineering, Stanford University, Stanford, California, USA.

[4]Department of Radiology, University of Utah, Salt Lake City, Utah, USA.

Grant sponsor: NIH; Grant numbers: 1 R01 HL075803-01, R01 EB002524-01, and 5 K08 CA112449; Grant sponsor: The Ben B. and Iris M. Margolis Foundation; Grant sponsor: Brigham Young University.

*Correspondence to: Neal K. Bangerter, Ph.D., 469 Clyde Building, Brigham Young University, Provo, UT 84602. E-mail: nealb@ee.byu.edu

Received 25 September 2010; revised 1 May 2011; accepted 8 June 2011.

DOI 10.1002/mrm.23076

Published online 28 October 2011 in Wiley Online Library (wileyonlinelibrary.com).

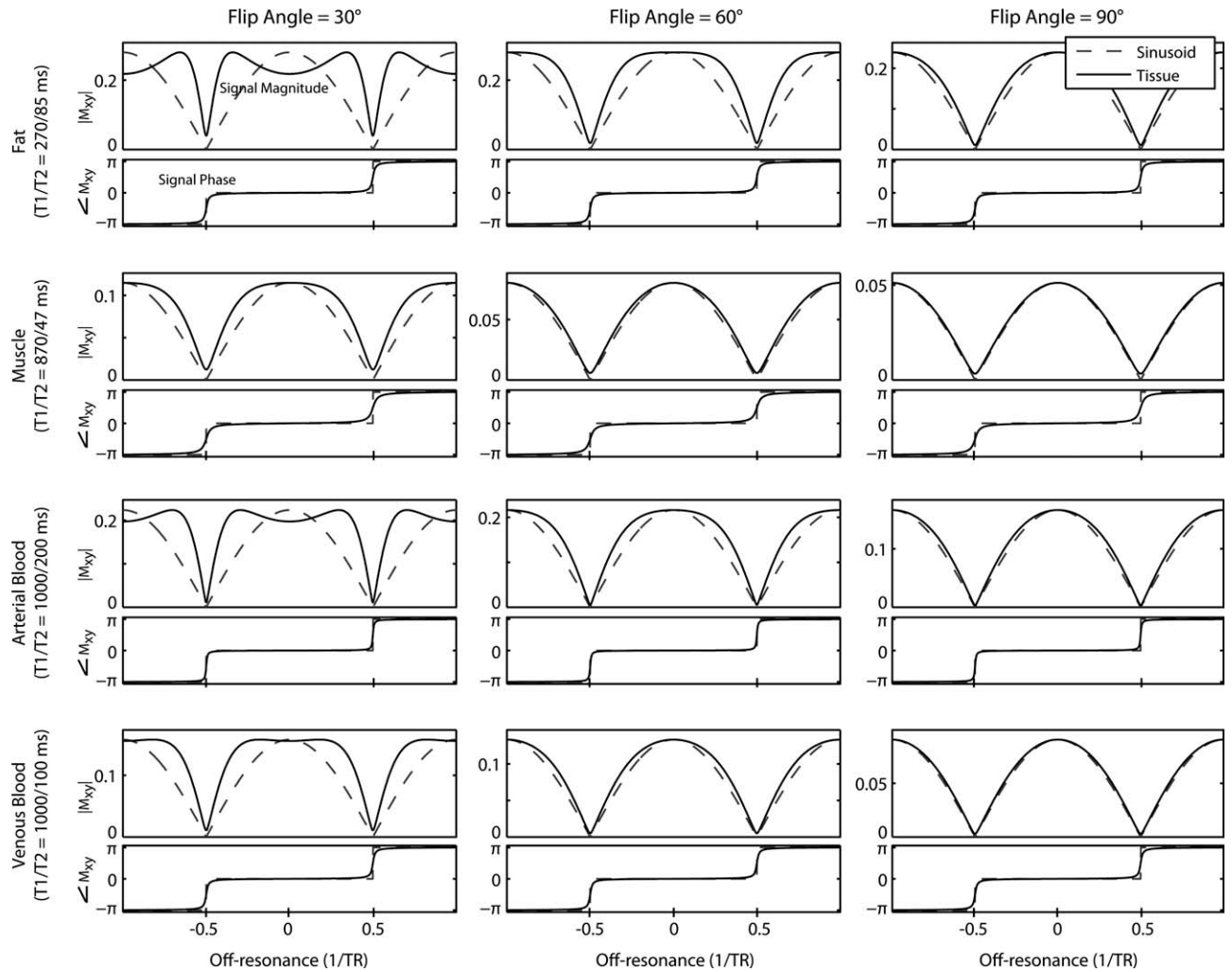

FIG. 1. The bSSFP signal as a function of off-resonance (solid line) is compared with a sinusoid (dashed line) for several tissues (fat, muscle, arterial blood, and venous blood) at flip angles of 30°, 60°, and 90°. As flip angle is increased, the bSSFP signal begins to more closely approximate a sinusoid for many tissues.

banding artifacts, works well at large flip angles, works in the presence of large field inhomogeneity, and keeps the scan time penalty to a minimum.

In this work, we present large-angle multiple-acquisition (LAMA) bSSFP, a novel bSSFP technique that simultaneously suppresses fat and reduces banding artifacts with the acquisition of only two phase-cycled bSSFP datasets. The technique relies on the near-sinusoidal shape of the bSSFP off-resonance spectrum for many tissues at large flip angle, and thus performs best under the large-flip-angle constraint of the flow-independent peripheral angiography application. Preliminary results are presented in both phantoms and in vivo, along with the results of a simulation and study assessing the performance of the technique across a range of flip angles.

THEORY

As the flip angle is increased, the bSSFP signal as a function of off-resonance frequency begins to approximate a sinusoid for many biological tissues (Fig. 1). (Note that this approximation strictly speaking requires echo time (TE) = TR/2. At other TE, a simple linear phase is introduced across the spectral profile, and the signal can be modeled by a complex exponential.) This spectral profile can be arbitrarily shifted in frequency by incrementing the phase of the radiofrequency pulse by some $\Delta\phi$ from excitation to excitation (3,4,7,8). When two large-flip-angle ($\sim$50° or greater) bSSFP acquisitions are performed with $\Delta\phi = 0°$ and 180°, the spectral profiles of the acquisitions approximate a sine and cosine, respectively, with period 2/TR Hz. A dataset with spectral profile shifted by a desired spectral shift Δf can then be synthesized from the two acquisitions, using the relationship

$$\sin[\pi \mathrm{TR}(f + \Delta f)] = \cos(\pi \mathrm{TR}\Delta f)\sin(\pi \mathrm{TR}f) + \sin(\pi \mathrm{TR}\Delta f)\cos(\pi \mathrm{TR}f), \quad [1]$$

as illustrated in Fig. 2.

Choice of TR such that TR = $n/(2 * \mathrm{CS_f})$, where n = [1, 3, 5, ...] and $\mathrm{CS_f}$ is the absolute chemical shift of fat relative to water (in Hz), will place fat in a signal null whenever water is at a signal maximum. Choice of TR to adjust the relative phase of fat and water is also

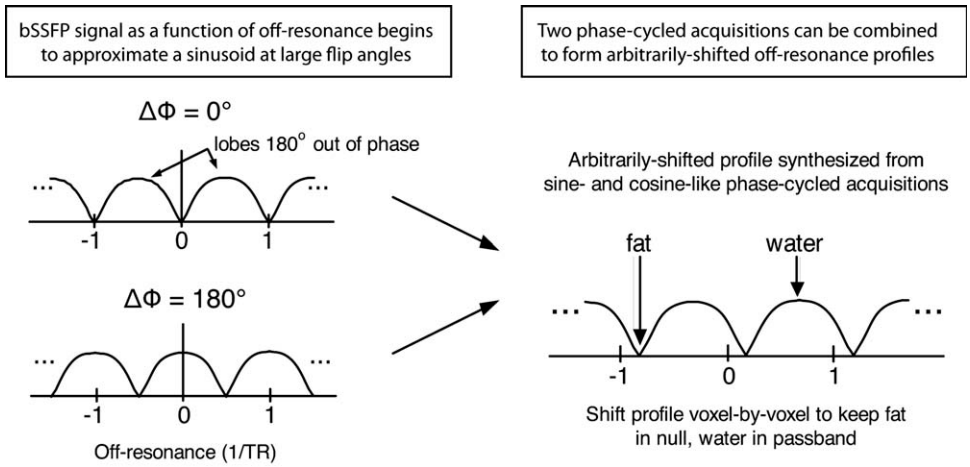

FIG. 2. Two large-angle phase-cycled acquisitions can be combined to synthesize an arbitrarily shifted bSSFP profile. An appropriate choice of TR allows fat to be placed in the signal null on a voxel-by-voxel basis.

exploited in Ref. 25. If the appropriate frequency shift Δf needed to place water on a signal maximum is then identified on a voxel-by-voxel basis, a fat-suppressed image without banding can theoretically be formed from just two phase-cycled acquisitions. This forms the basis for our LAMA bSSFP technique.

The required frequency shift for each voxel can be determined either through acquisition of a field map or through an intelligent search of voxel intensities over a range of Δf values (eliminating the need for field-map acquisition and the associated scan time penalty). In the latter case, a field map is essentially inferred by examining what values of Δf yield the maximum water and minimum fat signal for each voxel. When large jumps in these Δf values are observed in adjacent voxels, the voxels likely lie at a fat/water boundary. Region-growing algorithms can then be devised to identify voxels as predominantly fat or predominantly water, and a smooth map of Δf values synthesized.

Once a smooth Δf map is generated, water-only or fat-only images can be reconstructed. Let $S1_n$ be the complex signal of the nth voxel from the first phase-cycled acquisition (with $\Delta\phi = 0°$), $S2_n$ be the complex signal of the nth voxel from the second phase-cycled acquisition (with $\Delta\phi = 180°$), and Δf_n be the frequency shift required to put water in the center of the passband (and hence fat in the center of the null) for the nth voxel. The reconstructed signal intensity of the nth voxel in the water-only image (W_n) is then given by:

$$W_n = S1_n \cos(\pi \mathrm{TR} \Delta f_n) + S2_n \sin(\pi \mathrm{TR} \Delta f_n). \quad [2]$$

Similarly, the reconstructed signal intensity of the nth voxel in the fat-only image (F_n) is given by:

$$F_n = S1_n \sin(\pi TR \Delta f_n) - S2_n \cos(\pi TR \Delta f_n). \quad [3]$$

The above relations are clearly only valid, if the off-resonant spectral profiles of the tissues of interest are identically sinusoidal. Although the assumption of sinusoidal spectral profiles is an approximation, we can expect reasonable results across a range of tissues even at flip angles down to ~50°. In Fig. 3, the spectral profiles of several tissues (fat, arterial blood, venous blood, and muscle) at flip angles of 30°, 60°, and 90° are shown (first column). The second through fourth columns of Fig. 3 show spectral profiles synthesized from two phase-cycled acquisitions at Δf values of 1/(12TR), 1/(6TR), and 1/(4TR), respectively. Note that this range of Δf values spans the full range of distortion in the spectral profiles: the distortion at $\Delta f = 1/(3\mathrm{TR})$ is equivalent to that at 1/(6TR), and so forth. Although the profiles are distorted enough at a flip angle of 30° to suggest that the LAMA bSSFP method is impractical at these lower flip angles, the distortion is relatively mild at 60°, as illustrated in columns two through four of Fig. 3. The distortion continues to decrease for flip angles approaching 180° (irrespective of T_1/T_2), although signal attenuation becomes significant at flip angles approaching 180°.

The warping of synthesized profiles at different Δf values has an effect on signal contrast. An analysis of arterial/venous, arterial/muscle, and arterial/fat contrast (defined as the absolute signal difference between two tissues) is shown in Fig. 4 as a function of both flip angle and resonant shift Δf. As in Fig. 3, graphs are shown for $\Delta f = 0$, 1/(12TR), 1/(6TR), and 1/(4TR). Interestingly, the distortion tends to improve contrast between the relevant tissues for our flow-independent peripheral angiography application. T_1 and T_2 values assumed in all simulations for fat, muscle, arterial blood, and venous blood are listed in Table 1.

MATERIALS AND METHODS

Phantom and Lower Leg Data Acquisition

As an initial proof-of-concept, two phase-cycled bSSFP 3D images and a 3D field map were acquired of an oil/water phantom and the lower leg of a normal volunteer on a 1.5 T GE scanner (GE Healthcare, Waukesha, WI). All subject scans referenced in this work were conducted according to the guidelines of our Institutional Review Board. Scan parameters for the bSSFP acquisitions were: flip angle = 90° (phantom) and 70° (volunteer), TR/TE = 6.6/3.3 ms, and phase cycling of $\Delta\phi = 0°$ and 180°. Recall that TR for our technique is constrained to:

$$\mathrm{TR} = n/(2 * \mathrm{CS}_f), \quad \text{where } n = 1, 3, 5, \ldots \quad [4]$$

where $\mathrm{CS_f}$ is the absolute chemical shift of fat relative to water (in Hz). Assuming $\mathrm{CS_f} = 226$ Hz at 1.5 T, allowable

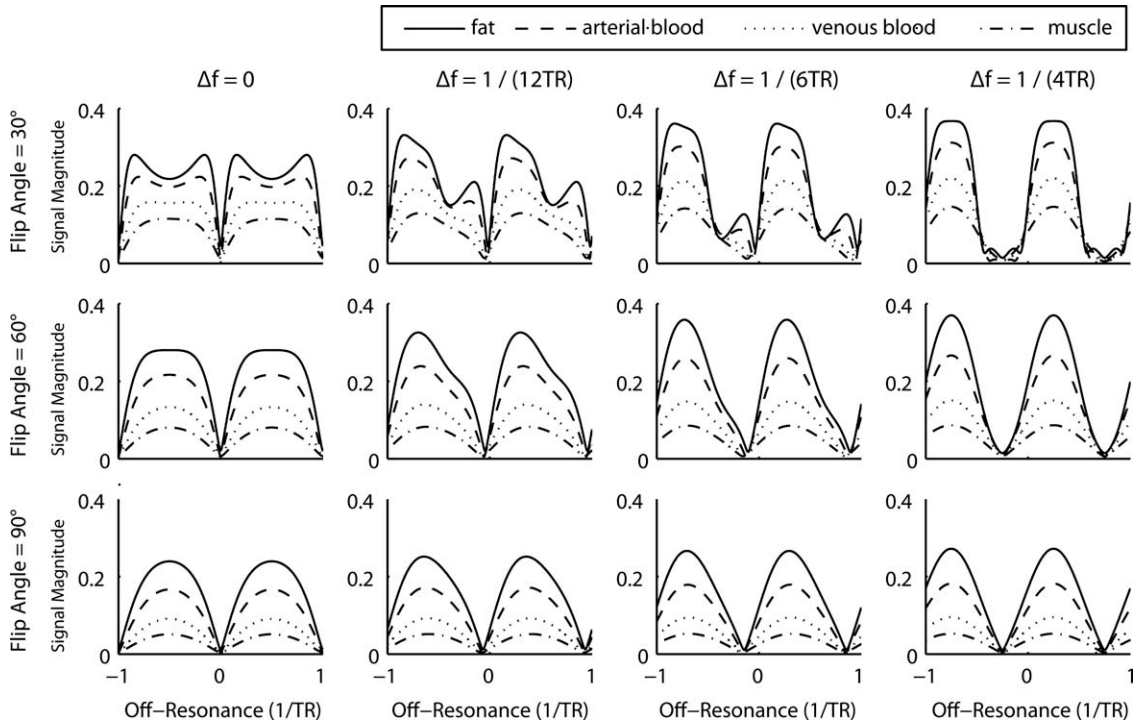

FIG. 3. Synthesized spectral profiles at different Δf values and different flip angles (α) created from two bSSFP phase-cycled data acquisitions with $\Delta\phi = 0^\circ$ and 180°, respectively. Note that the shape of the profiles are symmetric in Δf around 0 and 1/(4TR). As a consequence, the shape of synthesized profiles is only unique for Δf values from 0 to 1/(4TR). Spectra for Δf values of 0, 1/(12TR), 1/(6TR), and 1/(4TR) are shown above, representative of the full range of distortion in synthesized spectral profiles expected.

TRs are thus 2.2, 6.6, 11.1 ms, and so forth. A TR of 2.2 ms corresponds to placing fat in the null immediately adjacent to the water passband, and would be expected to be the most robust. However, a TR this short is difficult to achieve. Our choice of TR = 6.6 ms places fat in a null that is one removed from the water passband. A TR of greater than ~7 or 8 ms begins to be impractical for SSFP imaging because of the severity of off-resonance banding.

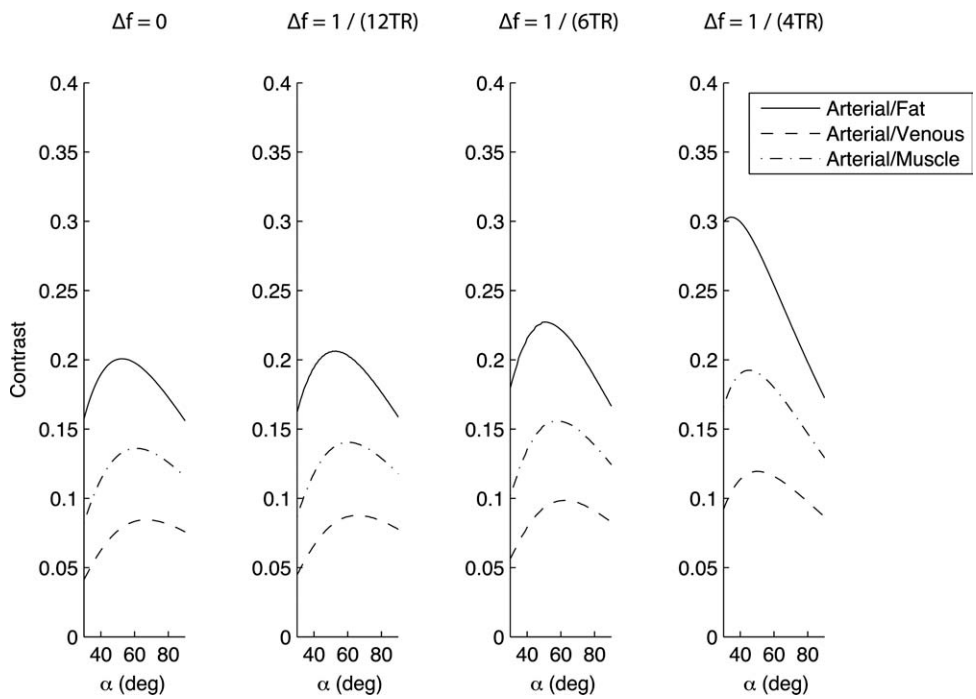

FIG. 4. The warping of synthesized profiles at different Δf values has an effect on signal contrast. An analysis of arterial/venous, arterial/muscle, and arterial/fat contrast is shown above as a function of both flip angle and resonant shift Δf. As in Figure 3, graphs are shown for $\Delta f = 0$, 1/(12TR), 1/(6TR), and 1/(4TR). Interestingly, the distortion tends to improve the contrast of the relevant tissues for the peripheral angiography application.

Table 1
T_1 and T_2 Values Assumed in Simulations for Muscle, Fat, Arterial Blood, and Venous Blood

Tissue	T_1 (ms)	T_2 (ms)
Muscle	870	47
Fat	270	85
Arterial blood	1000	200
Venous blood	1000	100

Values were informed by parameters found in Refs. 22, 26, and 27.

As mentioned, increasing TR spatially compresses bands of signal null, leading to more rapid spatial variations in signal and sharper band edges.

Field-Map Reconstruction

For field-map reconstruction, a field map was first acquired by taking the phase difference between two successive gradient-recalled echo (GRE) images with $\Delta TE = 1/CS_f$ (or 4.4 ms at 1.5 T). This ensures that fat and water voxels will be in phase for a voxel that has no off-resonance. The GRE images were acquired on the identical matrix as the bSSFP images. Then, the phase difference of each voxel within the image can be determined to calculate the off-resonance frequency for that voxel within a modulo of $1/\Delta TE$. The frequency Δf_n for the nth voxel was calculated by:

$$\Delta f_n = \Delta\theta_n/(2\pi\Delta TE) \quad [5]$$

where $\Delta\theta_n$ is the phase difference in radians of the nth voxel. Once Δf is known for each voxel and both bSSFP images have been acquired, the fat and water images can be created by inserting Δf_n into Eqs. 2 and 3.

Region-Growing Reconstruction

To eliminate the need for field-map acquisition, a region-growing algorithm was implemented that synthesizes a Δf-map using only the two phase-cycled bSSFP acquisitions. This map can be used in place of the field map.

The two constituent phase-cycled images are first processed by creating reconstructed sets of images, where each image is shifted by different values of Δf ranging from 0 to 1/TR. (Note that these values only span half of the period of the off-resonance spectra, as we are only concerned with the magnitude of the final image.) Afterward, the new set of images are scanned on a voxel-by-voxel basis to find Δf_{max} for each voxel, where Δf_{max} is defined as the Δf value that produces the maximum intensity for that voxel, A maximum-intensity image is also produced by selecting the maximum intensity found for each voxel across the new set of images. Voxels that are all fat or all water, at the same off-resonant frequency, will have Δf_{max} values that are separated in frequency by 1/(2TR).

In the peripheral angiography application, the brightest voxels are typically fat. Thus, the assumption is made that the brightest voxel in the maximum-intensity image is always going to be a fat voxel with little to no partial-volume effects. Thus, the algorithm assigns the Δf_{max} of that voxel to be Δf_{fat} and Δf_{water} to be $\Delta f_{fat} - 1/(2TR)$. Although this method performs reasonably well for our application, the identification of a fat pixel could be done manually by the MR operator if needed.

Once Δf_{fat} and Δf_{water} for the first voxel are determined, the Δf_{max} of each neighboring voxel is compared with the first voxel to determine if it is fat or water. If the Δf_{max} of the neighboring voxel is within a predefined threshold of the surrounding Δf_{fat} or Δf_{water} values, then the new voxel is identified as either fat or water and Δf_{fat} and Δf_{water} for that voxel are assigned accordingly. If the Δf_{max} is not close to the known neighboring Δf_{fat} or Δf_{water} values, the voxel is skipped and will not be identified as fat or water.

The algorithm continues in a region-growing fashion until no new neighbors can be identified as either fat or water across the entire dataset. Two slight modifications to the algorithm were found to be helpful in images with large field of view, low resolution, or less than ideal shims. The first modification involves adding magnitude thresholds to limit false identification for voxels close to the noise floor. The second modification is to only use pixels identified as fat for construction of the Δf-map, as these voxels typically have the highest SNR. In some situations, using only fat voxels proved to be more robust in avoiding misidentification in regions of large B_0 inhomogeneity.

Once the region-growing algorithm has identified Δf_{water} and Δf_{fat} for any identifiable voxels, Δf_{fat}-map and Δf_{water}-map are created by interpolating Δf_{water} and Δf_{fat} to fill in voxels that were unidentifiable. When only fat voxels are used, the Δf_{fat}-map is created first, and the Δf_{water}-map is synthesized by subtracting 1/(2TR) from the Δf_{fat}-map. The Δf_{fat}-map and Δf_{water}-map are then filtered to enforce only gradual off-resonance variation on pixels that were not originally identified. The original images are then reprocessed using the Δf_{water}-map to make a water-only image and Δf_{fat}-map to make a fat-only image.

Contrast and Performance Simulations

A simulation was performed to analyze the performance and contrast of LAMA bSSFP at different off-resonance values and at multiple flip angles. A 3D lower leg phantom was simulated in Matlab (The MathWorks, Natick, MA) by creating a volumetric dataset consisting of a tapered cylinder with fat on the surface and muscle in the middle. Fat pockets of different sizes were randomly placed in the muscle portion. A bifurcated artery and two veins were then added, running superior/inferior (vertically in the images presented). T_1 and T_2 values assumed for muscle, fat, arterial blood, and venous blood are listed in Table 1. A linear variation in resonant frequency was added to the simulated phantom, also in the vertical (superior/inferior) direction. The off-resonant shift ranged from $-1/TR$ in the most inferior portion of the simulated phantom to 1/TR in the most superior portion (-152 to $+152$ Hz based on TR = 6.6 ms).

Using this simulated phantom, the expected signal was simulated for two phase-cycled bSSFP acquisitions

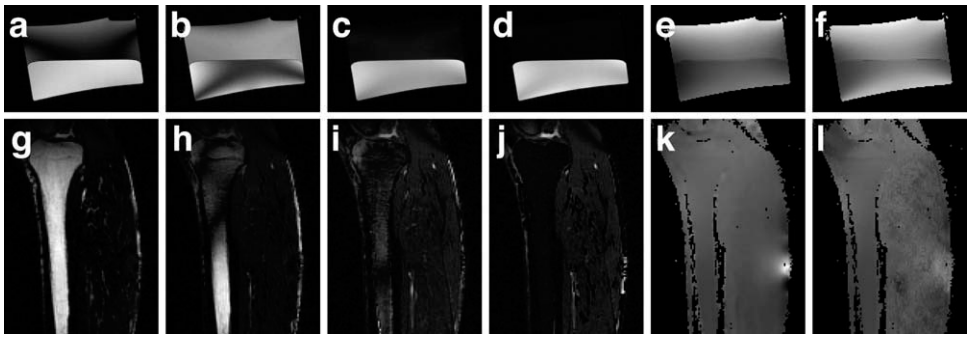

FIG. 5. Images from oil/water phantom (top) and lower-leg (bottom) experiments demonstrating LAMA bSSFP at 1.5 T. Regular bSSFP acquisitions are shown in (a) and (g) for $\Delta\phi = 0°$ and in (b) and (h) for $\Delta\phi = 180°$. LAMA bSSFP images using field-map reconstruction are shown in (c) and (i), and the corresponding images using the region-growing reconstruction are shown in (d) and (j). Fat is well suppressed using both LAMA reconstruction techniques, although a notable improvement is evident with the region-growing reconstruction method. For reference, the acquired field maps are shown in (e) and (k), and the maps synthesized using the region-growing algorithm are shown in (f) and (l).

at flip-angles of 30°, 40°, 50°, 60°, 70°, 80°, and 90°. Fat was assumed to be perfectly off-resonance at 226 Hz (the chemical shift at 1.5 T). Complex zero-mean gaussian noise was added with an SNR of 31.6. Then, these data were processed using the region-growing algorithm as described.

Contrast and Performance Verification In Vivo

To verify the contrast and performance simulation, 3D LAMA bSSFP images were acquired of a normal volunteer in vivo using a 1.5 T GE MRI scanner (GE Healthcare, Waukesha, WI) at flip angles of 30°, 50°, 70°, and 90°. Parameters were chosen assuming a CS_f of 226 Hz, such that TR = 6.6 ms and TE = 3.3 ms, and two datasets acquired at each flip angle with phase cycling of $\Delta\phi = 0°$ and 180°, respectively. Other parameters were: field of view = 28 × 14 × 14 cm and matrix size = 256 × 64 × 128.

RESULTS

Phantom and Lower Leg Data Acquisition

Individual phase-cycled 1.5 T acquisitions of both the oil/water phantom (Fig. 5a,b) and the lower leg of a normal volunteer (Fig. 5g,h) are shown. Banding is evident in both the phantom and the in vivo phase-cycled images. LAMA bSSFP water-only reconstructions using the acquired field maps are shown in Fig. 5c,i and exhibit relatively good fat suppression in both the phantom and the leg. However, fat suppression appears to be less robust in regions of large field inhomogeneity, such as in the subcutaneous fat. Furthermore, even in regions of relatively homogeneous field, fat suppression is less than optimal, possibly due to noise in the acquired field map.

LAMA bSSFP water-only images reconstructed using the region-growing algorithm are shown in Fig. 5d,j. The region-growing reconstruction effectively suppresses fat in both the phantom and the leg. While better than the field-map reconstruction, the region-growing reconstruction is still susceptible to misidentifications of fat in regions of large field inhomogeneity. Note that a small segment of subcutaneous fat was incorrectly identified as water, and hence not suppressed. In regions, where voxels were correctly identified as predominantly fat or water, fat/water separation is excellent. For reference, the acquired field maps are shown in Fig. 5e,k, and the maps synthesized using the region-growing algorithm are shown in Fig. 5f,l.

Contrast and Performance Simulations

Results of the contrast and performance simulations on the simulated lower leg phantom are shown in Fig. 6 for flip angles ranging from 30° to 90°. All of the images are maximum-intensity projections (MIPs) of the reconstructed 3D dataset. The LAMA bSSFP reconstruction using the region-growing algorithm is shown in the lower panes, whereas a simple root sum-of-squares reconstruction of the two phase-cycled datasets is shown in the upper panes for comparison. The simulated images highlight the improved fat suppression of LAMA bSSFP at larger flip angles. Smaller flip angles show regions, where the arterial/muscle contrast is less than ideal. The signal decreases from many tissues as the flip angle increases. Arterial/venous and arterial/muscle contrast (defined as the absolute signal difference between tissues) is maximized at flip angles of ~50–60°. Note that the region-growing algorithm performs very well in this simulation, given the enforced slow variation in field homogeneity.

Contrast and Performance Verification In Vivo

Results of the contrast and performance verification in vivo at 1.5 T are shown in Fig. 7 for flip angles of 30°, 50°, 70°, and 90°. As with the simulation results, all images are MIPs through the reconstructed 3D dataset. As expected, some fat suppression occurs at lower flip angles, but the fat-suppression performance of LAMA bSSFP improves as the flip angle is increased. Residual off-resonance signal modulations (banding) also decrease, as the flip angle is increased. The ability of the region-growing algorithm to correctly identify the frequency shift (and consequently to classify voxels as either fat or water) improves as the flip angle increases.

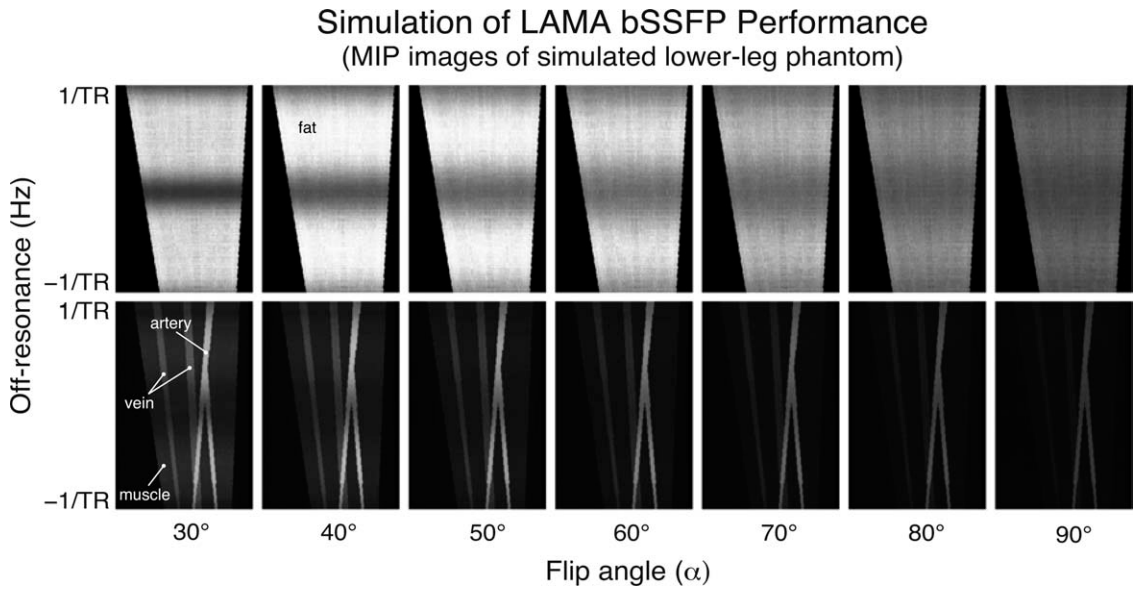

FIG. 6. Simulation of LAMA bSSFP contrast across a range of flip angles in a simulated 3D lower leg phantom. Two phase-cycled acquisitions of the 3D phantom were simulated, and then reconstructed using a simple root sum-of-squares reconstruction (top row) and the region-growing LAMA reconstruction technique (bottom row). The images shown are MIPs through each reconstructed 3D dataset. A linear off-resonant shift in the vertical (superior/inferior) direction was simulated to assess the performance of each method given variations in resonance frequency, and noise added to each phase-cycled dataset before reconstruction. Residual banding as a function of off-resonance is evident as signal modulations in the vertical direction. Off-resonance values vary from 1/TR to −1/TR (152 to −152 Hz for an assumed TR of 6.6 ms).

Less distortion is also expected in the reconstructed off-resonance profiles at larger flip angles, as demonstrated in Fig. 3. The in vivo results appear to correspond well with the results expected given the simulations presented in Fig. 6. However, focal signal loss that mimics pathology is evident in some areas. We suspect this arises from errors in the synthesis of the Δf-map, but a more thorough exploration of the source of these artifacts is needed.

DISCUSSION

There are several clear limitations of the LAMA bSSFP technique that should be addressed. First, the requirement of relatively large flip angles (greater than $\sim 50^\circ$), while reasonable for the flow-independent peripheral angiography work that motivated this research, could limit the utility of the method for other bSSFP applications. In many situations, lower flip angles are desired to maximize the bSSFP signal. Furthermore, the large-flip-angle requirement may lead to specific absorption rate considerations, particularly at higher field strengths.

The constraints imposed on TR by the LAMA bSSFP technique may also make it impractical for certain applications. As previously mentioned, TR must be chosen such that $TR = n/(2 * CS_f)$, where $n = 1, 3, 5, \ldots$ and CS_f is the absolute chemical shift of fat relative to water (in Hz). In practice, only TRs between ~ 2.5 and 10 ms are practical for most bSSFP applications. This limits choice of TR in the above equation to $n = 3$ for 1.5 T and $n = 5$ for 3 T. Although we have achieved good results at both 1.5 T (with $n = 3$) and 3 T (with $n = 5$), n values of greater than 5 are likely to result in poor performance for LAMA bSSFP, as both the fat null and the water passband become narrower in frequency and further removed from each other. At 7 T, we expect LAMA bSSFP to be largely impractical.

In this work, the coronal orientation was used such that blood flow is mainly along the readout (superior/inferior) direction, thus minimizing the impact of flow-dependent phase variations. Flow-dependent phase variations are expected to have an adverse impact on the performance of the LAMA bSSFP technique, as the technique relies on the predictable variations in signal phase arising from off-resonance. Further work is needed to understand the sensitivity of the technique to flow-induced phase.

As reported in the previous section, we were able to achieve better results with the region-growing reconstruction technique than using a field map to inform LAMA reconstruction. The region-growing synthesis results in a Δf-map that partially compensates for the distortions caused by the fact that off-resonance spectra are not truly sinusoidal. However, there is still significant room for improvement and optimization of the LAMA technique. We have experimented with several different filtering methods to enforce smoothness in the Δf-maps synthesized by the region-growing reconstruction method. Across regions with small and smooth variations in B_0, these filtered Δf-maps yield very good results. However (and not surprisingly), we have found that the region-growing technique achieves better fat suppression in regions of rapid B_0 variations when the filtering step is eliminated. Further work is needed to tailor and optimize LAMA bSSFP for various possible applications.

Synthesis of the Δf-map during region-growing reconstruction hinges on the successful classification of a

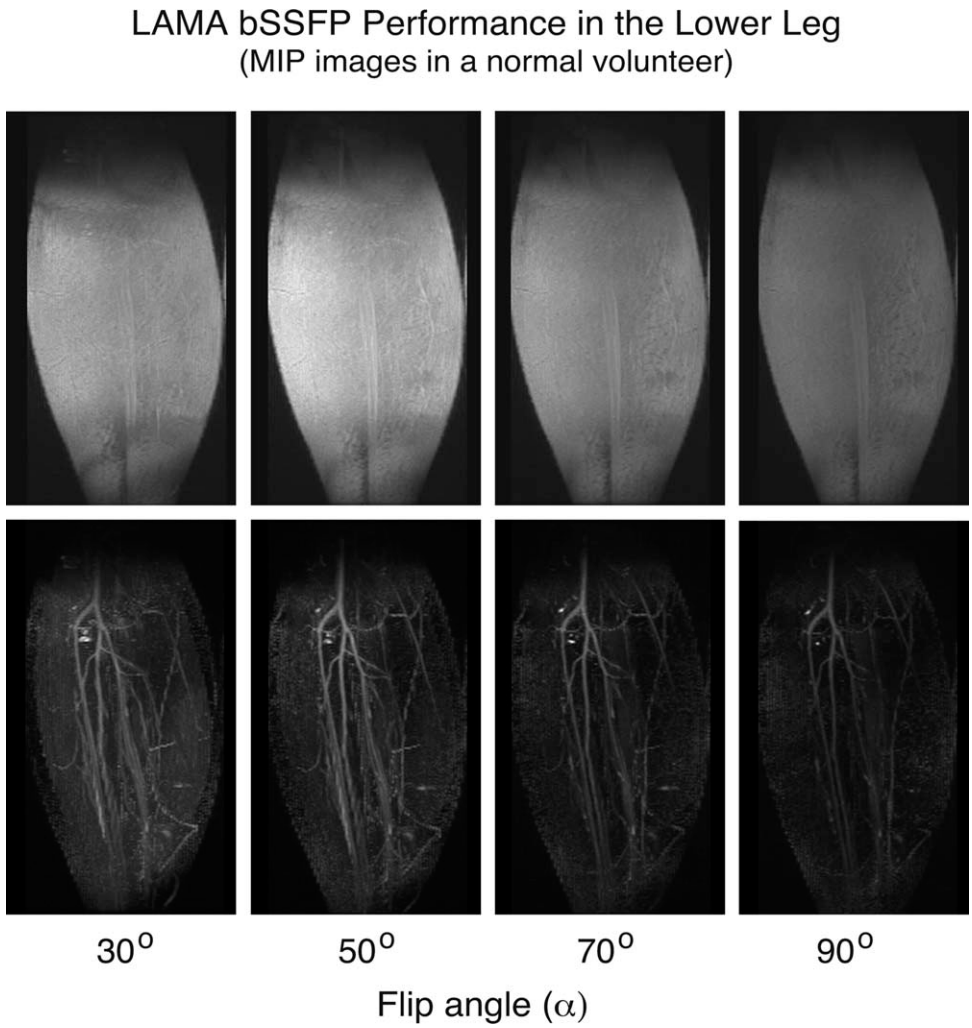

FIG. 7. Contrast and performance comparison of region-growing LAMA bSSFP in vivo at 1.5 T. Lower leg MIPs of a normal volunteer are shown using a standard root sum-of-squares reconstruction (top row) and the region-growing LAMA reconstruction technique (bottom row) across a range of flip angles. The better fat-suppression performance of LAMA bSSFP at larger flip angles is clearly evident, although the technique performs surprisingly well at flip angles down to 30°.

sufficient number of voxels to allow interpolation of the missing points. One reason this classification might fail is simply due to insufficient signal for that voxel. However, failure can also result from partial-volume effects (e.g., when a voxel has comparable signal contributions from both fat and water). A region-growing LAMA bSSFP reconstruction can fail, if too large a proportion of voxels split their volume across fat and water. Sometimes, we have observed this failure in muscle tissue with significant fat content. In these cases, a field-map-based reconstruction might perform more reliably.

Although partial-volume effects may cause synthesis of the Δf-map to fail, it is important to point out that the LAMA bSSFP technique is in general robust to partial-volume effects provided an accurate Δf-map is available. If the true off-resonance shift of a given voxel is known, fat signal from that voxel can be separated from water signal by the LAMA reconstruction technique. Thus, although partial-volume effects may result in synthesis of a poor Δf-map using a region-growing technique, they should not adversely affect a LAMA bSSFP reconstruction performed with an accurate Δf-map. However, it is important to note that the relatively broad fat spectrum with multiple peaks will still degrade the performance of the technique. Further work is needed to understand the magnitude of this degradation.

Future work will focus on optimization of the LAMA bSSFP technique for flow-independent peripheral angiography. A more detailed comparison and analysis of the Δf-maps synthesized from region-growing techniques versus those derived directly from a field map could help inform this optimization. In some cases, the small amount of time needed to perform a low-resolution field map for reconstruction may be a valid trade-off, if reconstruction is significantly improved. Hybrid techniques that use both a field map and a synthesized Δf-map could also be explored to make the technique more robust. Furthermore, a detailed analysis and comparison of the performance of the LAMA technique to other SSFP fat suppression and band-reduction techniques needs to be performed.

CONCLUSIONS

In summary, LAMA bSSFP is a novel technique that simultaneously suppresses fat and reduces bSSFP banding artifacts with the acquisition of only two phase-cycled bSSFP datasets and a field map (in the case of a

field-map-based reconstruction). Preliminary implementations have been demonstrated with promising results. In addition to the field-map-based reconstruction, a region-growing reconstruction that eliminates the need for field-map acquisition has been demonstrated at both field strengths successfully. The technique shows particular promise for flow-independent peripheral angiography using bSSFP, where large flip angles are desirable to achieve good vessel conspicuity. Further work is needed to fully optimize the proposed technique, compare its performance to other bSSFP techniques, and assess its applicability to other potential applications.

REFERENCES

1. Carr HY. Steady-state free precession in nuclear magnetic resonance. Phys Rev 1958;112:1693–1701.
2. Freeman R, Hill HDW. Phase and intensity anomalies in Fourier transform NMR. J Magn Reson 1971;4:366–383.
3. Schwenk A. NMR pulse techniques with high sensitivity for slowly relaxing systems. J Magn Reson 1971;5:376–389.
4. Hinshaw WS. Image formation by nuclear magnetic resonance: the sensitive point method. J Appl. Phys 1976;47:3709.
5. Oppelt A, Graumann R, Barfuss H, Fischer H, Hartl W, Shajor W. FISP—a new fast MRI sequence. Electromedica 1986;54:15–18.
6. Zur Y, Stokar S, Bendel P. An analysis of fast imaging sequences with steady-state transverse magnetization refocusing. Magn Reson Med 1988;6:175–193.
7. Haacke EM, Wielopolski PA, Tkach JA, Modic MT. Steady-state free precession imaging in the presence of motion: application for improved visualization of the cerebrospinal fluid. Radiology 1990; 175:545–552.
8. Zur Y, Wood ML, Neuringer LJ. Motion-insensitive, steady-state free precession imaging. Magn Reson Med 1990;16:444–459.
9. Bangerter NK, Hargreaves, BA, Vasanawala SS, Pauly JM, Gold GE, Nishimura DG. Analysis of multiple-acquisition SSFP. Magn Reson Med 2004;51:1038–1047.
10. Nayak KS, Hsu-Lei L, Hargreaves BA, Hu BS. Wideband SSFP: alternating repetition time balanced steady state free precession with increased band spacing. Magn Reson Med 2007;58:931–938.
11. Foxall DL. Frequency-modulated steady-state free precession imaging. Magn Reson Med 2002;48:502–508.
12. Vasanawala SS, Pauly JM, Nishimura DG. Linear combination steady-state free precession MRI. Magn Reson Med 2000;43:82–90.
13. Hennig J, Speck O, Scheffler K. Optimization of signal behavior in the transition to driven equilibrium in steady-state free precession sequences. Magn Reson Med 2002;48:801–809.
14. Vasanawala SS, Pauly JM, Nishimura DG. Fluctuating equilibrium MRI. Magn Reson Med 1999;42:876–883.
15. Reeder SB, Wen Z, Yu H, Pineda AR, Gold GE, Markl M, Pelc NJ. Multicoil Dixon chemical species separation with an iterative least-squares estimation method. Magn Reson Med 2004;51:35–45.
16. Reeder SB, Pineda AR, Wen Z, Shimakawa A, Yu H, Brittain JH, Gold GE, Beaulieu CH, Pelc NJ. Iterative decomposition of water and fat with echo asymmetry and least-squares estimation (IDEAL): application with fast spin-echo imaging. Magn Reson Med 2005;54: 636–644.
17. Huang TY, Chung HW, Wang FN, Ko CW, Chen CY. Fat and water separation in balanced steady-state free precession using the Dixon method. Magn Reson Med 2004;51:243–247.
18. Hargreaves BA, Vasanawala SS, Nayak KS, Hu BS, Nishimura DG. Fat-suppressed steady-state free precession imaging using phase detection. Magn Reson Med 2003;50:210–213.
19. Hargreaves BA, Bangerter NK, Shimakawa A, Vasanawala SS, Brittain JH, Nishimura DG. Dual-acquisition phases-sensitive fat-water separation using balanced steady-state free precession. Magn Reson Imaging 2006;24:113–122.
20. Cukur T, Nishimura DG. Fat-water separation with alternation repetition time balanced SSFP. Magn Reson Med 2008;60:479–484.
21. Scheffler K, Heid O, Hennig J. Magnetization preparation during the steady-state: fat-saturated 3D true FISP. Magn Reson Med 2001;45: 1075–1080.
22. Brittain JH, Olcott EW, Szuba A, Gold GE, Wright GA, Irarrazaval P, Nishimura DG. Three-dimensional flow-independent peripheral angiography. Magn Reson Med 1997;38:343–354.
23. Cukur T, Lee JH, Bangerter NK, Hargreaves BA, Nishimura DG. Non-contrast-enhanced flow-independent peripheral MR angiography with balanced SSFP. Magn Reson Med 2009;61:1533–1539.
24. Bangerter, NK. Contrast enhancement and artifact reduction in steady-state magnetic resonance imaging. Doctoral thesis, Stanford University, Palo Alto, CA, 2004.
25. Yu H, Reeder SB, Markl M, Pelc NJ. Single acquisition water fat separation for SSFP cardiac CINE imaging: feasibility study. In: Proceedings of the 12th Annual Meeting of ISMRM, Kyoto; 2004. p 263.
26. Wright GA, Hu BS, Macovski A. Estimating oxygen saturation of blood in vivo with MR imaging at 1.5 T. J Magn Reson Imaging 1991; 1:275–283.
27. Gronas R, Kalman PG, Kucey DS, Wright GA. Flow-independent angiography for peripheral vascular disease: initial in-vivo results. J Magn Reson Imaging 1997;7:637–643.